Vietnam Journal of Science and Technology ***58*** *(2) (2020) 152-161*

doi:10.15625/2525-2518/58/2/13929

STRUCTURAL, MAGNETIC AND ELECTRICAL PROPERTIES OF Ho AND Ni CO-DOPED $BiFeO_3$ MATERIALS[#]

Dao Viet Thang[1, 2, *], Nguyen Manh Hung[1, 2], Bui Thi Thu[2], Le Thi Mai Oanh[2], Bui Dinh Tu[3], Nguyen Van Minh[2]

[1]*Department of Physics, Hanoi University of Mining and Geology, 18 Vien Street, Duc Thang Ward, North Tu Liem District, Ha Noi, Viet Nam*

[2]*Center for Nano Science and Technology, Hanoi National University of Education, 136 Xuan Thuy Road, Cau Giay District, Ha Noi, Viet Nam*

[3]*Faculty of Engineering Physics and Nanotechnology, VNU-University of Engineering and Technology, 144 Xuan Thuy Road, Cau Giay District, Ha Noi, Viet Nam*

[*]Email: *daovietthang@humg.edu.vn*

Received: 10 July 2019; Accepted for publication: 2 December 2019

Abstract. Pure $BiFeO_3$ (BFO) and $Bi_{1-x}Ho_xFe_{0.97}Ni_{0.03}O_3$ (x = 0, 0.025, 0.05, 0.075, and 0.1) materials were synthesized by a sol-gel method. The influence of (Ho, Ni) co-doping on structural, magnetic and electrical properties of BFO materials were investigated by different techniques as X-ray diffraction (XRD), energy dispersion X-ray (EDX), Raman scattering, magnetic hysteresis (*M-H*) loops, and complex impedance spectra measurement. XRD results showed that all samples were crystallized in the rhombohedral structure with R_{3C} space group. Crystal lattice parameters (a, c) and average crystal size L_{XRD} were (a = 5.584 Å, c = 13.867 Å, L_{XRD} = 60 nm) for pure BFO, (a = 5.589 Å, c = 13.875 Å, L_{XRD} = 60 nm) for $BiFe_{0.97}Ni_{0.03}O_3$ sample, and then decreased with increasing of Ho content in (Ho, Ni) co-doped samples. Similarly, Raman scattering spectra showed the left shift of active modes Fe-O bonds when doping Ni and right shift when co-doping Ho. These observations confirmed the successful substitution of Ho^{3+} and Ni^{2+} ions into the host BFO crystal lattice. Magnetic hysteresis loops measurement indicated that all samples exhibited weak ferromagnetic behavior with saturation magnetization M_s and remnant magnetization M_r of (M_s ~ 0.047 emu/g, M_r ~ 0.008 emu/g) for pure BFO which increased gradually for (Ho, Ni) co-doped samples, reached to (M_s ~ 0.702 emu/g, M_r ~ 0.169 emu/g) for x = 0 sample. Origin of the enhancement of ferromagnetization in (Ho, Ni) co-doped samples have been discussed.

Keywords: X-ray, Raman, (Ho, Ni) co-doped, ferromagnetic, impedance.

Classification numbers: 2.2.1, 2.2.2.

1. INTRODUCTION

[#] Presented at the 11th National Conference on Solid State Physics & Materials Science, Quy Nhon 11-2019.

Multiferroic materials, possessing simultaneously ferromagnetic (antiferromagnetic), ferroelectric and ferroelasticity orders, and magnetoelectric (ME) effect in the same structure phase, which have been reported by many previous studies [1-4]. Multiferroic can be used in electronic devices such as information storage, memory, sensor, and ultrasonic broadcast. Due to competition between ferromagnetic and ferroelectric orders, multiferroic are very rare in nature. $BiFeO_3$ (BFO) is one of multiferroic materials coexisting antiferromagnetic order (with Néel temperature T_N = 643 K) and ferroelectric order (with Curie temperature T_C = 1100 K) [3, 5]. However, BFO has small saturation magnetization M_s and polarization P_s which limits its applications. This problem can be solved by modification of magnetic and electrical properties of BFO. Studies have shown that ferromagnetism and ferroelectricity of BFO can be improved by substitution of rare earth ions (Sm^{3+}, Nd^{3+}, Gd^{3+}, Ho^{3+}, etc.) into Bi-sites [6-8] or transition metal ions (Ni^{2+}, Co^{2+}, Mn^{2+}, etc.) into Fe-sites [9-11] or co-doping rare earth and transition metal [12-14]. Chakrabarti *et al*. [15] and Zhang *et al*. [16] indicated that magnetization of (Eu, Co) or (La, Co) co-doped BFO enhanced several times compared to that of BFO. Ye *et al*. [17] showed that both ferromagnetic and ferroelectric properties of (Ho, Mn) co-doped BFO were improved compared to that of BFO.

In this work, holmium (Ho) and nickel (Ni) will be co-doped into BFO. Since the appropriate content of 2 ÷ 3 molar% of Ni^{2+} dopant was demonstrated in several studies for largest enhancing of multiferroics properties [13, 18, 19], Ni^{2+} concentration in co-doped samples will be kept at a constant of 3 molar%. The content of Ho^{3+} ions changes in the range of 0 ÷ 10 molar% to study the effect of (Ho, Ni) co-doping on structural and physical properties of BFO.

2. MATERIALS AND METHOD

Pure $BiFeO_3$ and $Bi_{1-x}Ho_xFe_{0.97}Ni_{0.03}O_3$ (x = 0, 0.025, 0.05, 0.075, and 0.1) materials were synthesized by sol-gel method. The chemicals used were: bismuth nitrate pentahydrate $Bi(NO_3)_3.5H_2O$ (Sigma-Aldrich, 98.0 %), iron nitrate nonahydrate $Fe(NO_3)_3.9H_2O$ (Sigma-Aldrich, 98 %), holmium nitrate pentahydrate $Ho(NO_3)_3.5H_2O$ (Sigma-Aldrich, 99.99 %), nickel nitrate hexahydrate $Ni(NO_3)_2.6H_2O$ (Sigma-Aldrich, 99.99 %), ethylene glycol solution $C_2H_6O_2$ (China, 99 %), and citric acid $HOC(COOH)(CH_2COOH)_2$ (China, 99.5 %). The $Bi(NO_3)_3.5H_2O$, $Fe(NO_3)_3.9H_2O$, $Ho(NO_3)_3.5H_2O$, and $Ni(NO_3)_2.6H_2O$ were dissolved in 35 ml citric acid solution 1 M. The solution was then mixed by magnetic stirring at temperature of 60 °C for 45 minutes to obtain a reddish-brown transparent solution. Then, temperature of the sol was increased up to 100 °C for 3 hours to evaporate and obtain wet gel. Next, the gel was dried at 130 °C for 4 hours. Finally, dry gel was annealed at temperature 800 °C for 7 hours to obtain powder materials.

The microstructure, magnetic and electrical properties of all samples were investigated by using X-ray diffraction (XRD, Equinox 5000, Cu-$K\alpha$ radiation), energy dispersive X-ray spectrometry (EDX, Quanta 450), Raman scattering (LabRAM HR Evolution, λ = 532 nm), scanning electron microscopy images (SEM, Quanta 450), magnetization hysteresis loops (*M-H*, Lake Shore Cryotronics, 7404 VSM), and complex impedance measurement (LeCroy equipment with range frequency from 10 Hz to 5.3 MHz and LabView 8.0 software).

For the measurements of complex impedance, powder materials were compressed by a pressure of 20 MPa into round tablets of 6 mm in diameter and 1 mm thick. The round tablets were sintered at temperature of 800 °C for 5 hours to obtain ceramics. Then, the ceramic tablets were polished after measuring accurately their thickness. Finally, the samples were evenly covered with Pt glue as electrode and sintered at temperature of 500 °C for 3 hours.

3. RESULTS AND DISCUSSION

The chemicals composition of pure BFO and $Bi_{1-x}Ho_xFe_{0.97}Ni_{0.03}O_3$ (x = 0, 0.05 and 0.1) powders investigated by EDX spectra measurement are shown in Fig. 1. As seen in Fig. 1, EDX spectra of all samples exhibit characteristic peaks for Bi, Fe, and O elements. EDX spectrum of BFNO presents one more peak at 7.42 eV corresponding to Ni element while that of (Ho, Ni) co-doped samples show two more characteristic peaks for Ho element at 1.35 eV and 6.64 eV. The intensity of Ho characteristic peaks increases as increasing Ho content.

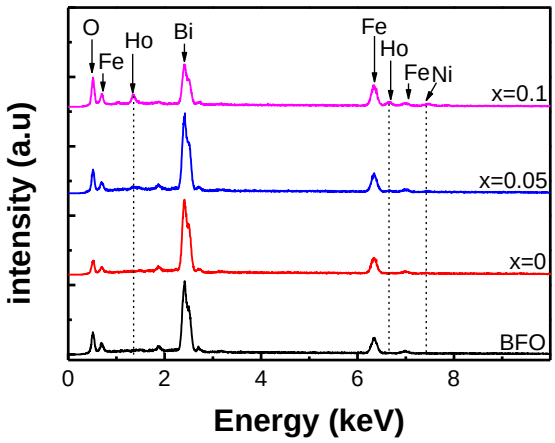

Figure 1. EDX spectra of $BiFeO_3$ and $Bi_{1-x}Ho_xFe_{0.97}Ni_{0.03}O_3$ (x = 0, 0.05, and 0.1) powders.

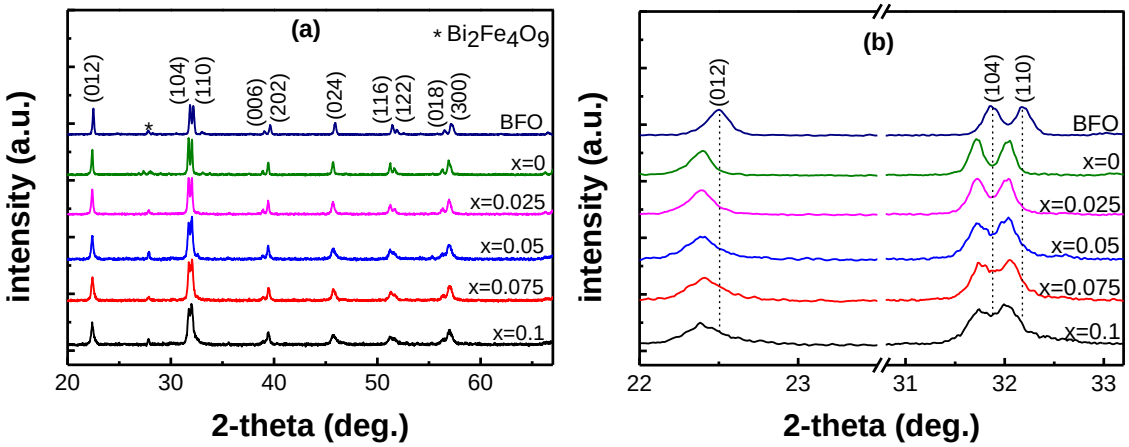

Figure 2. XRD patterns of $BiFeO_3$ and $Bi_{1-x}Ho_xFe_{0.97}Ni_{0.03}O_3$ (x = 0, 0.025, 0.05, 0.075, and 0.1) powders.

XRD patterns recorded in order to investigate phase formation and crystal structure of as synthesized materials are shown in Fig. 2a. The XRD patterns reveal that all synthesized samples crystallized in rhombohedral structure of $BiFeO_3$ crystal (JPCDS No. 71-2494) with lattice planes as (012), (104), (110), (006), (202), (024), (116), (122), (018), and (300). The XRD patterns of BFNO and (Ho, Ni) co-doped samples show that Ho^{3+} and Ni^{2+} ions were well dissolved into the BFO host lattice without the appearance of strange peaks. Fig. 2b displays a comparison of the location of (012), (104), and (110) diffraction peaks which shows that these

peaks shift obviously toward the lower 2θ angle when doping Ni^{2+} ions and then shift slightly to the higher 2θ angle when co-doping Ho^{3+} ions. Lattice parameters (a and c) and average crystal size (L_{XRD}) have been determined by using UnitCell software and Debye Scherrer's formula (Table 1). As seen in Table 1, the lattice parameters (a = 5.584 Å, c = 13.867 Å) for BFO sample increase to (a = 5.589 Å, c = 13.875 Å) for BFNO sample and then decrease gradually with increasing Ho content. This change can be assigned to difference of ionic radius between Ni^{2+} (0.69 Å) and Fe^{3+} (0.65 Å) ions as well as the difference of ionic radius between Ho^{3+} (1.02 Å) ions and Bi^{3+} (1.17 Å) ions. Small ionic radius of Ho^{3+} is not enough to fill 12-sided cavity created by BO_6 octahedron, resulting to the rotation of the BO_6 octahedron (B is Fe or Ni) and the reduction of the volume of 12-sided cavity. For (Ho, Ni) co-doped samples with high Ho content, the rotation of BO_6 octahedron is large enough to reduce both a and c parameters as observed in Table 1. Part *et al.* [18] also suggested that the change in lattice parameters originated from the fact that ionic radius of Ho^{3+} is smaller than that of Bi^{3+} and the ionic radius of Ni^{2+} is larger than that of Fe^{3+}.

Table 1. Crystal lattice parameters and average crystal size of $BiFeO_3$ and $Bi_{1-x}Ho_xFe_{0.97}Ni_{0.03}O_3$ (x = 0, 0.025, 0.05, 0.075, and 0.1) samples.

Samples	a (Å)	c (Å)	L_{XRD} (nm)
BFO	5.584	13.867	60
x = 0	5.589	13.875	60
x = 0.025	5.588	13.873	50
x = 0.050	5.588	13.868	42
x = 0.075	5.586	13.863	37
x = 0.1	5.582	13.857	33

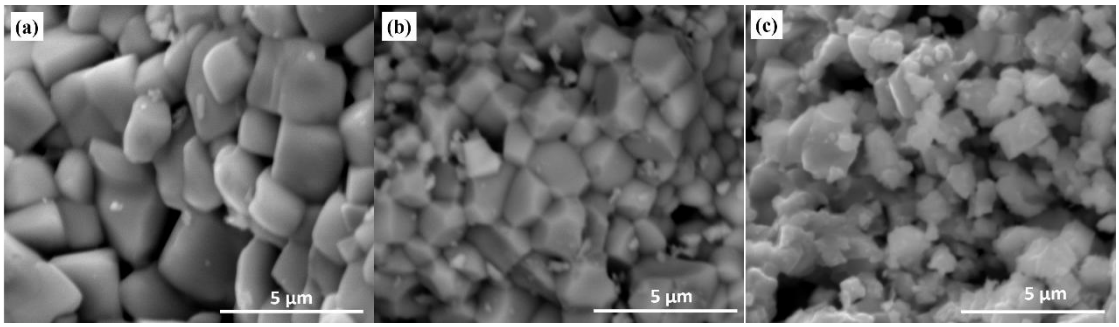

Figure 3. SEM images of BFO and $Bi_{1-x}Ho_xFe_{0.97}Ni_{0.03}O_3$ samples: (a) BFO; (b) x = 0; and (c) x = 0.1.

Figure 3 shows scanning electron microscope (SEM) images of $BiFeO_3$ and $Bi_{1-x}Ho_xFe_{0.97}Ni_{0.03}O_3$ (x = 0, and 0.1) samples. BFO sample consists of granular particles with a fairly large size of about a few micrometers (Fig. 3a) and clear boundary. When doping Ni^{2+} into Fe^{3+} site, the particle size decreases obviously and becomes more inhomogeneous (Fig. 3b). The particle size decreases further to less than 1 micrometer when co-doping Ho^{3+} into Bi^{3+} site (Fig. 3c). Furthermore, particles size and morphology are poorly homogeneous. In particular, the grain boundary becomes less clear. This reveals that Ni^{2+} doping and (Ni^{2+}, Ho^{3+}) co-doping affect strongly on the particle size and morphology of $BiFeO_3$ which also can be attributed to the

differences of doping ions (Ni^{2+}, Ho^{3+}) and host lattice ions (Fe^{3+}, Bi^{3+}). The substitution of these doping ions in BFO lattice leads to a certain disorder in crystal structure, resulting to restrict the crystalline growth.

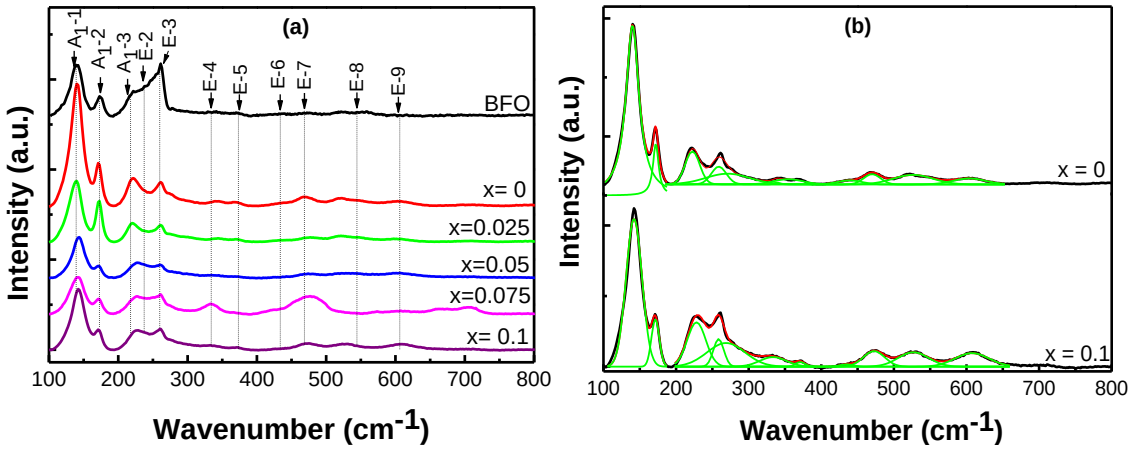

Figure 4. (a) Raman scattering spectra of $BiFeO_3$ and $Bi_{1-x}Ho_xFe_{0.97}Ni_{0.03}O_3$ (x = 0, 0.025, 0.05, 0.075, and 0.1) materials; (b) Fitted Raman peaks in the wavenumber region of 100 to 800 cm^{-1}.

Raman scattering spectra of BFO and $Bi_{1-x}Ho_xFe_{0.97}Ni_{0.03}O_3$ are shown in Fig. 4a. According to the group theory, 13 Raman active modes could be desirable for the rhombohedral BFO structure with R_{3C} space group ($\Gamma = 4A_1 + 9E$) [20, 21]. However, not all modes could be clearly observed at room temperature [22]. Raman peaks of all samples are fitted by Gaussian function, as are shown in Fig. 4b and Table 2.

Table 2. The Raman modes positions of $BiFeO_3$ and $Bi_{1-x}Ho_xFe_{0.97}Ni_{0.03}O_3$ (x = 0, 0.025, 0.05, 0.075, and 0.1) materials (cm^{-1}).

Modes	BFO	x = 0	x = 0.025	x = 0.05	x = 0.075	x = 0.1
A_1-1	139	140	138	143	141	142
A_1-2	173	171	172	171	172	171
A_1-3	225	223	222	228	227	228
E-2	252	258	257	258	258	258
E-3	262	278	296	280	279	272
E-4	285	344	344	340	334	334
E-5	336	369	372	370	365	371
E-6	433	434	435	437	424	437
E-7	474	470	477	472	475	473
A_1-4	521	517	518	530	571	527
E-8	555	547	539	605	607	607
E-9	706	604	602	655	668	689

As seen in Table 2, for the x = 0 sample, positions of A_1-1, A_1-2, A_1-3, A_1-4, E-6, E-7 modes change a little, position of E-2, E-3, E-4 and E-5 modes shift toward higher frequency while E-8

and *E*-9 modes shift toward lower frequency in comparison with those of BFO. For the (Ho, Ni) co-doped samples, positions of A_1-1, A_1-3, A_1-4, *E*-3, *E*-6, and *E*-7 modes tend to shift slightly toward higher frequency, positions of *E*-2, *E*-4, and *E*-5 modes change a little, while positions of *E*-8 and *E*-9 modes tend to shift strongly toward higher frequency in comparison with those of the $x = 0$ sample. Previous studies have also showed that the A_1 modes and *E* modes at low frequency characterize for Bi-O covalent bonds, other *E* modes at high frequency characterize for Fe-O bonds [23]. The A_1-1, A_1-3, A_1-4, *E*-3, *E*-6, and *E*-7 modes characterize for Bi-O covalent bonds [14, 24], while the *E*-8, *E*-9 modes characterize for Fe-O bonds [11, 25]. So the changes of *E*-8, *E*-9 modes confirmed Ni^{2+} ions substituted into Fe-sites, and the changes of A_1-1, A_1-2, A_1-3, A_1-4, *E*-3, *E*-6 and *E*-7 confirmed Ho^{3+} ions substituted into Bi-sites. These results are conformable to the XRD results, which confirmed that Ho^{3+} and Ni^{2+} ions substituted into Bi-sites and Fe-sites, respectively.

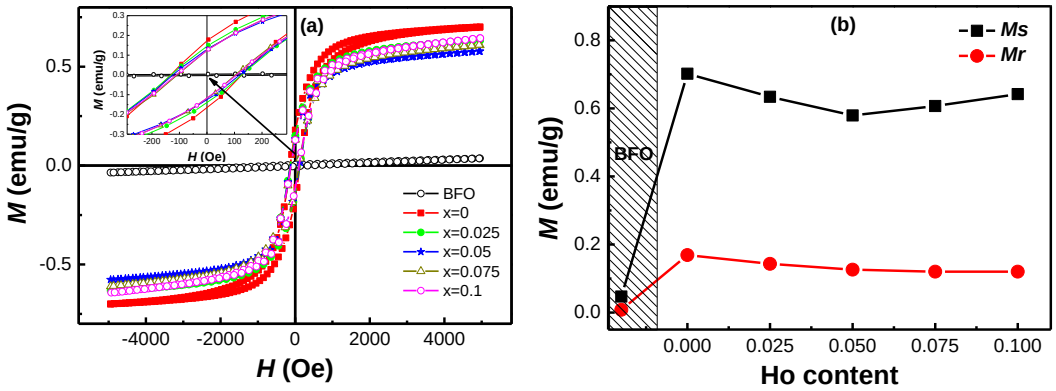

Figure 5. (a) Magnetic hysteresis loops of $BiFeO_3$ and $Bi_{1-x}Ho_xFe_{0.97}Ni_{0.03}O_3$ materials; (b) Dependence of saturation magnetization and remnant magnetization on concentration of Ho.

Figure 5a shows magnetic hysteresis loops of BFO and $Bi_{1-x}Ho_xFe_{0.97}Ni_{0.03}O_3$ materials at room temperature. As seen in Fig. 5a, all samples present weak ferromagnetic behavior. BFO sample has saturation magnetization of $M_s = 0.047$ emu/g and remanent magnetization of $M_r = 0.008$ emu/g. When doping with Ni^{2+} ions in Fe^{3+} site, M_s and M_r values increase to 0.702 emu/g and 0.169 emu/g, respectively. However, when co-doping Ho^{3+} in Bi^{3+} site they decrease slightly as observed in Fig. 5b. This reveals that Ni^{2+} doping enhances ferromagnetization in BFO that can be attributed to some following reasons: (i) the appearance of ferrimagnetic order Ni^{2+}-O^{2-}-Fe^{3+} besides antiparallel indirect interaction between Fe^{3+} and neighbor Fe^{3+} [26, 27]; (ii) Ni^{2+} replacement in Fe^{3+} site causes the charge shortage, in order to neutralize the charge, some Fe^{3+} ions transform to Fe^{4+}, resulting the ferromagnetic double exchange interaction Fe^{3+}-O^{2-}- Fe^{4+}; (iii) the enhancement of magnetization due to the appearance of oxygen vacancies and lattice defects when doping Ni^{2+} in BFO lattice [28]. The slight decrease of saturation magnetization and remanent magnetization in (Ho, Ni) co-doped samples in Fig. 5b could be explained by the reduction of oxygen vacancies due to Bi^{3+} volatilization [29, 30]. However, the M_s and M_r values in (Ho, Ni) co-doped samples are still larger 12 and 15 times in comparison with those of BFO.

Figure 6 shows complex impedance spectra of $BiFeO_3$ and $Bi_{1-x}Ho_xFe_{0.97}Ni_{0.03}O_3$ ($x = 0$, 0.05, and 0.1) which can indicate the contribution of grain, grain boundaries, and electrode interface into impedance of materials. As can be seen, simulated curves fit well with the experimental curves in all samples. Fig. 6a presents that the impedance spectrum of BFO

consists of one semicircle at high frequency and one semicircle at intermediate frequency, which indicate the contribution of grains and grain boundaries, respectively. The resistance of grain boundaries is much larger than that of grains. Figs. 6b, c, d exhibit only one semicircle that corresponds to the contribution of grain. As observed in XRD and SEM results, particle size was large for BFO and then decreased obviously when doping Ni^{2+} and co-doping Ho^{3+} into BFO. Furthermore, the grain boundary became less clear after doping Ni^{2+} and co-doping Ho^{3+}. This may be the reason for the contribution of grains and grain boundaries into impedance of samples. Since the limitation of frequency range, the contribution of electrode interface to impedance can't be detected in all samples.

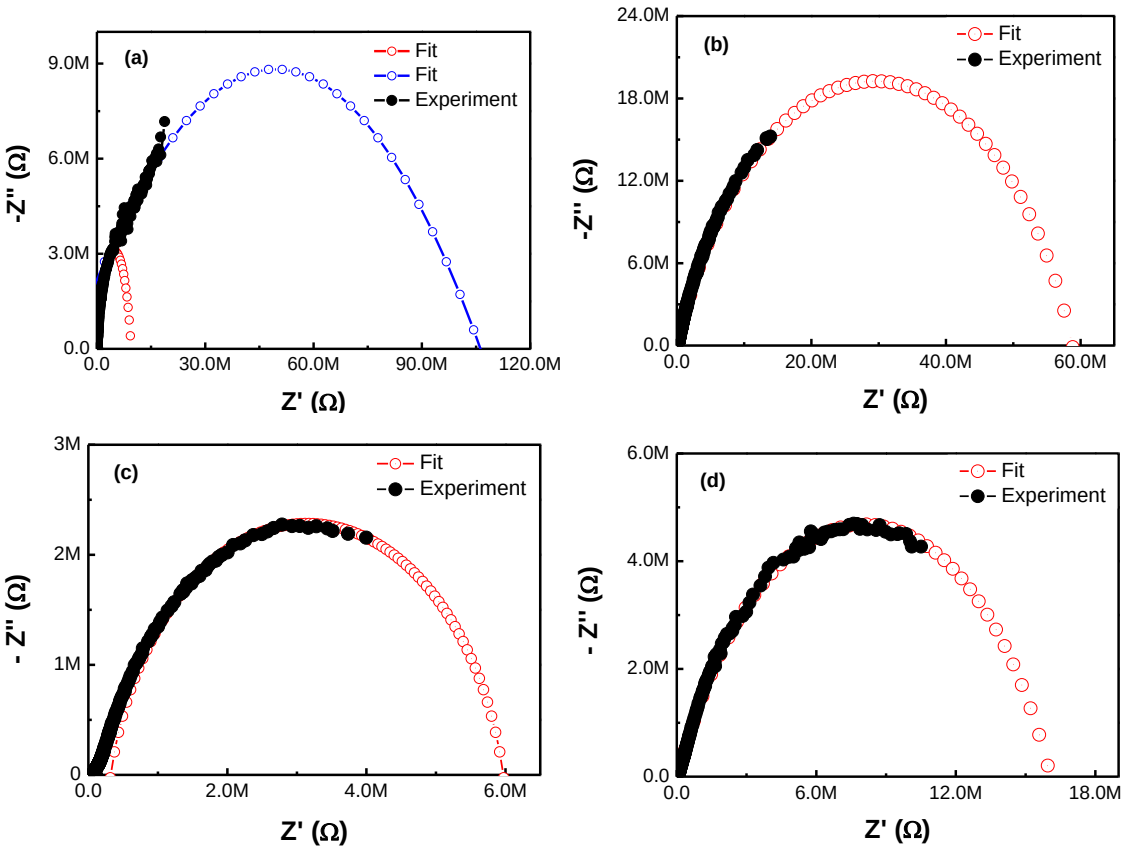

Figure 6. Impedance spectra of $BiFeO_3$ (a) and $Bi_{1-x}Ho_xFe_{0.97}Ni_{0.03}O_3$ materials with x = 0 (b), x = 0.05 (c), and x = 0.1 (d).

4. CONCLUSION

In summary, $BiFeO_3$ and $Bi_{1-x}Ho_xFe_{0.97}Ni_{0.03}O_3$ (x = 0, 0.025, 0.05, 0.075, and 0.1) materials have been successfully fabricated by sol-gel method. All samples crystallize in rhombohedral structure of BFO materials. Crystal lattice parameters and average crystallite size increased with doping Ni^{2+} and decreased gradually with co-doping Ho^{3+}. X-ray diffraction patterns and Raman scattering spectra confirmed the successful substitution of Ho^{3+} and Ni^{2+} ions into Bi-sites and Fe-sites, respectively, which affected obviously to magnetic and electrical properties of BFO. Ni^{2+} replacement kept an important role in enhancing ferromagnetization of BFO. Complex

impedance spectra showed the main contribution of grains and grain boundaries into impedance of samples.

Acknowledgement. This work has been supported by the Ministry of Education and Training of Vietnam (Code B2018-MDA-02-CtrVL).

REFERENCES

1. Eerenstein W., Mathur N. D. and Scott J. F. - Multiferroic and magnetoelectric materials, Nature **442** (2006) 759-765.
2. Ederer C. and Spaldin N. A. - Weak ferromagnetism and magnetoelectric coupling in bismuth ferrite, Phys. Rev. B **71** (2005) 060401(R).
3. Ravindran P., Vidya R., Kjekshus A., Fjellvåg H. and Eriksson O. - Theoretical investigation of magnetoelectric behavior in $BiFeO_3$, Phys. Rev. B **74** (2006) 224412.
4. Cheong S. W. and Mostovoy M. - Multiferroics: a magnetic twist for ferroelectricity, Nat. mater. **6** (2007) 13-20.
5. Bhide V. G. and Multani M. S. - Mössbauer effect in ferroelectric-antiferromagnetic $BiFeO_3$, Solid State Commun. **3** (1965) 271-274.
6. Kumarn M., Sati P. C., Chhoker S. and Sajal V. - Electron spin resonance studies and improved magnetic properties of Gd substituted $BiFeO_3$ ceramics, Ceram. Int. **41** (2015) 777–786.
7. Zhang X., Sui Y., Wang X., Wang Y. and Wang Z. - Effect of Eu substitution on the crystal structure and multiferroic properties of $BiFeO_3$, J. Alloy. Compd. **507** (2010) 157-161.
8. Pradhan S. K., Das J., Rout P. P., Mohanta V. R., Das S. K., Samantray S., Sahu D. R., Huang J. L., Verma S. and Roul B. K. - Effect of holmium substitution for the improvement of multiferroic properties of $BiFeO_3$, J. Phys. Chem. Solids **71** (2010) 1557-1564.
9. Naganuma H., Miura J. and Okamura S. - Ferroelectric, electrical and magnetic properties of Cr, Mn, Co, Ni, Cu added polycrystalline $BiFeO_3$ films, Appl. Phys. Lett. **93** (2008) 052901.
10. Dai Y. R., Xun Q., Zheng X., Yuan S., Zhai Y. and Xu M. - Magnetic properties of Ni-substituted $BiFeO_3$, Physica B **407** (2012) 560–563.
11. Dong G., Tan G., Luo Y., Liu W., Ren H. and Xia A. - Optimization of the multiferroic $BiFeO_3$ thin films by divalent ion (Mn, Ni) co-doping at B-sites, Mater. Lett. **118** (2014) 31-33.
12. Viet Thang D., Thi Mai Oanh L., Cao Khang N., Manh Hung N., Danh Bich D., Thi Xuan Thao D. and Van Minh N. - Structural, magnetic and electric properties of Nd and Ni co-doped $BiFeO_3$ materials, AIMS Mater. Sci. **4** (2017) 982-990.
13. Thang D. V., Hung N. M., Thao D. T. X., Oanh L. T. M., Bich D. D., Khang N. C., Nguyen V. Q. and Minh N. V. - Structural, Electrical, and Magnetic Properties of $Bi_{0.90}Nd_{0.10}Fe_{0.98}TM_{0.02}O_3$ (TM = Mn, Co, Ni, and Cu) Materials, IEEE Mag. Lett. **10** (2019) 2501505.
14. Yan X., Tann G., Liu W., Ren H. and Xia A. - Structural, electric and magnetic properties of Dy and Mn co-doped $BiFeO_3$ thin film, Ceram. Int. **41** (2015) 3202–3207.

15. Chakrabarti K., Das K., Sarkar B., Ghosh S. and De S. K. - Enhanced magnetic and dielectric properties of Eu and Co co-doped $BiFeO_3$ nanoparticles, Appl. Phys. Lett. **101** (2012) 042401.
16. Zhang X., Zhang C. and Ran N. - Tailoring the magnetic and optical characteristics of $BiFeO_3$ ceramics by doping with La and Co, Mater. Lett. **179** (2016) 186-189.
17. Ye W., Tann G., Dong G., Ren H. and Xia A. - Improved multiferroic properties in (Ho, Mn) co-doped $BiFeO_3$ thin films prepared by chemical solution deposition, Ceram. Int. **41** (2015) 4668–4674.
18. Park J. S., Yoo Y. J., Hwang J. S., Kang J. H., Lee B. W. and Lee Y. P. - Enhanced ferromagnetic properties in Ho and Ni co-doped $BiFeO_3$ ceramics, J. Appl. Phys. **115** (2014) 013904.
19. Rajput S. S., Katoch R., Sahoo K. K., Sharma G. N., Singh S. K., Gupta R. and Garg A. - Enhanced electrical insulation and ferroelectricity in La and Ni co-doped $BiFeO_3$ thin film, J. Alloy.Compd. **621** (2015) 339–344.
20. Hermet P., Goffinet M., Kreisel J. and Ghosez P. - Raman and infrared spectra of multiferroic bismuth ferrite from first principles, Phys. Rev. B **75** (2007) 220102.
21. Luo L., Wei W., Yuan X., Shen K., Xu M. and Xu Q. - Multiferroic properties of Y-doped $BiFeO_3$, J. Alloy. Compd. **540** (2012) 36-38.
22. Huang J.-Z., Shen Y., Li M. and Nan C.-W. - Structural transitions and enhanced ferroelectricity in Ca and Mn co-doped $BiFeO_3$ thin films, J. Appl. Phys. **110** (2011) 094106.
23. Yuan G. L., Or S. W. and Chan H. L. - Raman scattering spectra and ferroelectric properties of $Bi_{1-x}Nd_xFeO_3$ (x = 0-0.2) multiferroic ceramics, J. Appl. Phys. **101** (2007) 064101.
24. Gautam A., Singh K., Sen K., Kotnala R. K. and Singh M. - Crystal structure and magnetic property of Nd doped $BiFeO_3$ nanocrytallites, Mater. Lett. **65** (2011) 591-594.
25. Arora M., Sati P. C., Chauhan S., Kumar M. and Chhoker S. - Structural, magnetic and optical properties of Ho–Co codoped $BiFeO_3$ nanoparticles, Mater. Lett. **132** (2014) 327-330.
26. Yu L., Deng H., Zhou W., Zhang Q., Yang P. and Chu J. - Effects of (Sm, Mn and Ni) co-doping on structural, optical and magnetic properties of $BiFeO_3$ thin films fabricated by a sol-gel technique, Mater. Lett. **170** (2016) 85-88.
27. Iyyappa Rajan P., Mahalakshmi S. and Chandra S. - Establishment of half-metallicity, ferrimagnetic ordering and double exchange interactions in Ni-doped $BiFeO_3$ – A first-principles study, Comp. Mater. Sci. **130** (2017) 84-90.
28. Xue X., Tan G., Dong G., Liu W. and Ren H. - Studies on structural, electrical and optical properties of multiferroic (Ag, Ni and In) codoped $Bi_{0.9}Nd_{0.1}FeO_3$ thin films, Appl. Surf. Sci. **292** (2014) 702-709.
29. Kim Y. J., Kim J. W., Raghavan C. M., Oak J. J., Kim H. J., Kim W. J., Kim M. H., Song T. K. and Kim S. S. - Enhancement of electrical properties of (Gd, V) co-doped $BiFeO_3$ thin films prepared by chemical solution deposition, Ceram. Int. **39** (2013) S195-S199.
30. Pradhan S. K. and Roul B. K. - Effect of Gd doping on structural, electrical and magnetic properties of BiFeO3 electroceramic, J. Phys. Chem. Solids **72** (2011) 1180-1187.